C.P. No. 943

C.P. No. 943

MINISTRY OF TECHNOLOGY

AERONAUTICAL RESEARCH COUNCIL

CURRENT PAPERS

A Theoretical Investigation of the Effect of Aspect Ratio on Axial Flow Compressor Performance

By

J. H. Horlock and G J. Fahmi

LONDON: HER MAJESTY'S STATIONERY OFFICE

1967

SIX SHILLINGS NET

C.P. No.943*

May, 1966

A Theoretical Investigation of the Effect of Aspect Ratio on Axial Flow Compressor Performance

- By -
J. H. Horlock and G. J. Fahmi

SUMMARY

The performance of axial flow compressors is known to be affected by the choice of aspect ratio (the ratio of blade height to axial chord length). An analysis of the inviscid, incompressible flow in axial compressors of different aspect ratios is given in this paper. The main analysis is based on actuator disc theory, but a comparison is made between calculations based on this theory and the more recently developed streamline curvature analysis. This comparison shows close agreement between the calculations based on the two theories.

List of Contents

1./

---

*Replaces A.R.C.28 187.

1. Introduction

The performance of single-stage and multi-stage axial flow compressors has been observed to be adversely affected by an increase of aspect ratio (blade length to half stage length). This deterioration in performance appears to be related to a reduction in the operating range of individual blade rows which results in a lower surge pressure ratio in multi-stage compressors.

Such differences in performance of compressors with different aspect ratios have been known to exist for some time, but the published literature on this subject is limited. Some experiments which show the effect of aspect ratio in two-dimensional cascade tests have been reported[1,2], but these tests have mainly been carried out at design point incidence and have not been extended into the stall region. Most of the multi-stage compressor tests on the effect of aspect ratio have been obtained by aircraft engine companies and have not been published.

Several suggestions have been made to explain this "aspect ratio" effect - differences in the three-dimensional axisymmetric flow, variations in the secondary and tip clearance flows, the differing performance of the blade rows acting as diffusers of different aspect ratios. It has even been suggested that the effect is a simple Reynolds number one, since compressor tests with low aspect ratio are usually made at the same blade speed and blade height, but larger chord[3]. However it appears that differences in performance exist even when the Reynolds number is maintained constant as the aspect ratio is changed. No firm conclusion on the dominant effect has yet been drawn.

In this paper an attempt is made to investigate the first of the effects listed above - the change in the three-dimensional axisymmetric flows with variation of aspect ratio, using actuator-disc theory. In the course of the investigation, calculations based on actuator-disc theory have been compared with calculations based on "streamline curvature" analysis, first suggested by Smith, Traugott and Wislicenus[4] and developed by the research establishments and the engine companies (L. H. Smith, General Electric, W. Stubner, Pratt and Whitney, J. Ringrose, National Gas Turbine Establishment, R. Hetherington, Rolls Royce Ltd.). A programme developed at Rolls Royce by Hetherington and Silvester was used in the comparison given in this paper.

Three different examples were calculated - a single-stage compressor (high and low hub/tip ratio), a two-stage compressor and a multi-stage compressor (both with high hub/tip ratio). The aspect ratio was varied in each of these three examples, but the blade design (of the "exponential" type) was similar.

2. Analysis

2.1 General - The actuator-disc analysis is developed here for single-, two- and multi-stage compressors, excluding all losses due to annulus wall boundary layers and associated secondary flows. The problem is reduced to one of three-dimensional axisymmetric, incompressible, inviscid flow. The limitations of this approach are recognised, but since it is known that "aspect-ratio" effects occur in compressors in which there are relatively small changes in annulus area, it is considered that the present simplified approach, of studying the three-dimensional axisymmetric effects alone in an annulus with cylindrical walls, is justified.

Solution/

Solution of the flow equations, at and off design, involves setting up differential equations for the axial velocity that would exist far downstream of each blade row, if radial equilibrium were attained. Essentially, the tangential vorticity, the radial gradient of this "infinity" velocity distribution, is obtained.

The differential equation is obtained from the Bragg-Hawthorne expression

$$\frac{dh_o}{d\psi} = \frac{1}{r^2}\left(\eta r + \frac{\Theta d\Theta}{d\psi}\right). \qquad \ldots(1)$$

If it is supposed that radial displacements are small, that the flow deviates but little from a free vortex and that the gradients in stagnation pressure are also small then the tangential vorticity remains unchanged at a given radius downstream of the i^{th} disc (see Ref. 5). Hence

$$\eta_{\theta i} = \eta_{ie} = \eta_i = \frac{dC_{xi}}{dr} \qquad \ldots(2)$$

where θi, ie, i refer to locations immediately downstream of the disc, at the trailing edge, and at the imaginary "far downstream" location respectively.

The tangential velocity is controlled at the trailing edge and also remains unchanged at a given radius between the discs[5].

$$C_{\theta oi} = C_{\theta ie} = C_{\theta i}.$$

For the design problem C_θ is specified, and in this case for "exponential" blading,

$$C_{\theta ie} = a + \frac{b}{R} \qquad \text{downstream of rotor}$$

$$C_{\theta(i+1)e} = a - \frac{b}{R} \qquad \text{downstream of stator} \qquad \ldots(3)$$

where a and b are constants.

For the off-design case, α_{ie} and $\beta_{(i+1)e}$ are specified so that

$$C_{\theta ie} = U - C_{xie}\tan\beta_{ie} \qquad \text{downstream of rotor}$$

$$C_{\theta(i+1)e} = C_{x(i+1)e}\tan\alpha_{(i+1)e} \qquad \text{downstream of stator.} \qquad \ldots(4)$$

In the solution of both design and off-design problems, the Bragg-Hawthorne equation (1) is linearised by writing $d\psi = C_{xi} r\, dr$.

Substitution/

Substitution of (2) and (3) or (2) and (4) into (1) then gives the differential equation for C_{xi},

$$C_{xi}\frac{dC_{xi}}{dr} + \frac{C_{\theta ie}}{r}\frac{d(rC_{\theta ie})}{dr} = \frac{dh_{oie}}{dr}. \qquad \ldots(5)$$

2.2 The design problem

For the design problem, in which there are no gradients of stagnation enthalpy, equal work being done at all radii, the equation for axial velocity becomes

$$\frac{d}{dr}\left(\frac{C_x^2}{2}\right) + \frac{(a \pm \frac{b}{R})}{r}\frac{d}{dr}\left[\left(a \pm \frac{b}{R}\right)r\right] = 0. \qquad \ldots(6)$$

The "infinity" axial velocities are then obtained analytically (see Ref. 6) and the trailing-edge velocity distribution from interference equations of the form

$$C_{xie} = C_{xi} - \left(\frac{C_{xi} - C_{xi-1}}{2}\right)e^{-\pi\frac{x}{\ell}} + \left(\frac{C_{xi+1} - C_{xi}}{2}\right)e^{-\pi\frac{x}{\ell}} \qquad \ldots(7)$$

allowing for interference effects from adjacent discs only. (It is shown in Ref. 7 that if the first root only of the actuator disc equations for the perturbation in axial velocity is being taken, then it is justifiable to consider interference effects from adjacent rows only.)

The design angles are then deduced from

$$\tan\alpha = \frac{a - \frac{b}{R}}{C_{xie}} \qquad \text{for a stator}$$

$$\tan\beta = \frac{U - (a + \frac{b}{R})}{C_{xie}} \qquad \text{for a rotor.} \qquad \ldots(8)$$

This method of design was used for the single-stage and the two-stage compressors (both with hub/tip ratio = 0·750). For the multi-stage design (U.S.F.) the i^{th} rotor exit air angle was as that for the second-stage rotor, and the i^{th} stator exit air angle was as that for the first-stage stator.

It was assumed that the angle distributions with radius were unchanged "off-design", at all flow coefficients. These distributions are given in Appendix 4.

2.3/

2.3 The off-design problem

For the off-design case equation (5) has to be solved directly at the trailing edge of a stationary row, say the i^{th} row. The tangential components of the velocity "C_θ" are given by equation (4), with the flow angles now known from the design calculations of Section 2.2.

Again the axial velocity is given by an equation such as (7), or,

$$C_{xie} = \bar{\alpha}_i C_{xi} + \bar{\beta}_i C_{xi-1} + \bar{\gamma}_i C_{xi+1} \qquad \ldots(9)$$

where $\bar{\alpha}$, $\bar{\beta}$, $\bar{\gamma}$ are constants and $i = 1, 2, 3 \ldots\ldots$

Three cases are considered below, a single-stage, a two-stage and a multi-stage machine.

2.3.1 The single-stage compressor

2.3.1.1 High hub/tip ratio (0·750)

The first example considered is that of a single-stage axial flow compressor - an inlet guide vane row followed by a rotor row followed by a stator row - of hub/tip ratio 0·750.

Each row of blades is replaced by an actuator disc placed at mid-chord of the blades, and the tangential velocity is controlled at a trailing-edge location midway between the actuator discs, i.e., it is assumed that the blade rows have the same axial chord and the axial clearance is zero.

For the three rows the three equations to be solved become:

for the guide vane

$$C_{x_1} \frac{dC_{x_1}}{dr} + \frac{(\bar{\alpha}_1 C_{xo} + \bar{\beta}_1 C_{x_1} + \bar{\gamma}_1 C_{x_2})}{r} \tan \alpha_{1e}$$

$$\frac{d}{dr}(r(\bar{\alpha}_1 C_{xo} + \bar{\beta}_1 C_{x_1} + \bar{\gamma}_1 C_{x_2})\tan \alpha_{1e}) = 0 \qquad \ldots(10)$$

for the rotor

$$C_{x_2} \frac{dC_{x_2}}{dr} + \frac{[U - (\bar{\beta}_2 C_{x_1} + \bar{\gamma}_2 C_{x_2} + \bar{\delta}_2 C_{x_3})\tan \beta_{2e}]}{r}$$

$$\frac{d}{dr}\{r[U - (\bar{\beta}_2 C_{x_1} + \bar{\gamma}_2 C_{x_2} + \bar{\delta}_2 C_{x_3})\tan \beta_{2e}]\} =$$

$$\frac{d}{dr}[U - (\bar{\beta}_2 C_{x_1} + \bar{\gamma}_2 C_{x_2} + \bar{\delta}_2 C_{x_3})\tan \beta_{2e}$$

$$- (\bar{\alpha}_1 C_{xo} + \bar{\beta}_1 C_{x_1} + \bar{\gamma}_1 C_{x_2})\tan \alpha_{1e}] \qquad \ldots(11)$$

for/

for the stator

$$C_{x_3}\frac{dC_{x_3}}{dr}+\frac{(\bar{\gamma}_3 C_{x_2}+\bar{\delta}_3 C_{x_3})}{r}\tan\alpha_{3e}\frac{d}{dr}[r(\bar{\gamma}_3 C_{x_2}+\bar{\delta}_3 C_{x_3})\tan\alpha_{3e}]$$

$$=\frac{d}{dr}[U-(\bar{\beta}_2 C_{x_1}+\bar{\gamma}_2 C_{x_2}+\bar{\delta}_2 C_{x_3})\tan\beta_{2e}-(\bar{\alpha}_1 C_{x_0}+\bar{\beta}_1 C_{x_1}+\bar{\gamma}_1 C_{x_2})\tan\alpha_{1e}]. \quad \ldots(12)$$

In non-dimensional form these equations become

$$\begin{aligned} a_{11}V_1+a_{12}V_2+D_1 &= 0\\ a_{21}V_1+a_{22}V_2+a_{23}V_3+D_2 &= 0 \quad \ldots(13)\\ a_{31}V_1+a_{32}V_2+a_{33}V_3+D_3 &= 0 \end{aligned}$$

where

$$V_1=\frac{d}{dR}\left(\frac{C_{x_1}}{C_{x_0}}\right)$$

$$V_2=\frac{d}{dR}\left(\frac{C_{x_2}}{C_{x_0}}\right)$$

$$V_3=\frac{d}{dR}\left(\frac{C_{x_3}}{C_{x_0}}\right)$$

and a_{ij}, D_i are functions of non-dimensional radius $R=\frac{r}{r_t}$, C_{x_1}, $f_i=\tan(\alpha_{or}\beta)_{ie}$, $F_i=\frac{d}{dR}(f_i)$ and aspect ratio A.R.

A complete statement of the equations is given in Appendix 1.

2.3.1.2 Low hub/tip ratio (0·555)

The problem of a low hub/tip ratio single-stage axial flow compressor was also considered. Solutions of the equations were carried out in a similar fashion to that in the previous section. Flow angles at exit from a row were obtained from the design of the high hub/tip ratio stage by means of extrapolation.

2.3.2 The two-stage compressor

The next example considered is that of a two-stage, five row compressor-inlet guide vanes, first rotor, first stator, second rotor, second stator. Again all rows are replaced by actuator discs located at mid-chord of the blades and interference effects due to adjacent discs only are considered. Five equations are derived for the "infinity" distributions of axial velocity.

The/

The general form of these equations is

$$\begin{aligned}
a_{11}V_1 + a_{12}V_2 \qquad\qquad\qquad\qquad + D_1 &= 0 \\
a_{21}V_1 + a_{22}V_2 + a_{23}V_3 \qquad\qquad + D_2 &= 0 \\
a_{31}V_1 + a_{32}V_2 + a_{33}V_3 + a_{34}V_4 \qquad + D_3 &= 0 \qquad \ldots(14) \\
a_{42}V_2 + a_{43}V_3 + a_{44}V_4 + a_{45}V_5 + D_4 &= 0 \\
a_{52}V_2 + a_{53}V_3 + a_{54}V_4 + a_{55}V_5 + D_5 &= 0.
\end{aligned}$$

A complete statement of these equations is given in Appendix 2.

2.3.3 The multi-stage compressor (ultimate steady flow)

Finally, actuator-disc theory is applied to obtain the flow through a stage in a multi-stage machine in which the stage is deeply embedded, i.e., there are many similar stages both upstream and downstream. In the actuator-disc analysis this stage is replaced by two actuator discs, and the flow entering the stage is identical to that leaving the stage.

The equation for the axial velocity that would exist in radial equilibrium upstream of the rotor disc is

$$C_{xs}\frac{dC_{xs}}{dr} + \frac{C_{\theta se}}{r}\frac{d}{dr}(r\,C_{\theta se}) = \frac{dh_{os}}{dr}. \qquad \ldots(15)$$

The equation for the equilibrium axial velocity that would exist downstream of the rotor disc is

$$C_{xR}\frac{dC_{xR}}{dr} + \frac{C_{\theta Re}}{r}\frac{d}{dr}(r\,C_{\theta Re}) = \frac{dh_{oR}}{dr}. \qquad \ldots(16)$$

Downstream of the stator disc and upstream of the rotor disc of the next stage

$$C_{xs}\frac{dC_{xs}}{dr} + \frac{C_{\theta se}}{r}\frac{d}{dr}(r\,C_{\theta se}) = \frac{d}{dr}(h_{os} + \Delta W) \qquad \ldots(17)$$

since the velocity distributions are the same at entry to and exit from the stage

and $$h_{oR} = h_{os} + \Delta W.$$

From (15) and (17)

$$\frac{d}{dr}(\Delta W) = 0. \qquad \ldots(18)$$

But/

But

$$\Delta W = \Omega r(C_{\theta Re} - C_{\theta se})$$

then

$$\frac{d}{dr}(r\,C_{\theta se}) = \frac{d}{dr}(r\,C_{\theta Re}) \qquad \ldots(19)$$

or

$$\frac{d}{dr}(rC_{xse}\tan\alpha_e) = \frac{d}{dr}(U - C_{xe}\tan\beta_e)$$

and

$$r(C_{\theta Re} - C_{\theta se}) = r(U - C_{xRe}\tan\beta_e - C_{xse}\tan\alpha_e)$$

$$= \text{Constant.} \qquad \ldots(20)$$

From equation (15) and (16)

$$C_{xs}\frac{dC_{xs}}{dr} + \frac{C_{\theta se}}{r}\frac{d}{dr}(rC_{\theta se}) = C_{xR}\frac{d}{dr}C_{xR} + \frac{C_{\theta Re}}{r}\frac{d}{dr}(rC_{\theta Re}). \qquad \ldots(21)$$

From equation (19) and (21)

$$C_{xs}\frac{dC_{xs}}{dr} - C_{xR}\frac{dC_{xR}}{dr} = \left\{\frac{C_{\theta Re} - C_{\theta se}}{r}\right\}\frac{d}{dr}(rC_{\theta se}) \qquad \ldots(22)$$

$$= \left(\frac{U - C_{xRe}\tan\beta_e - C_{xse}\tan\alpha_e}{r}\right)\frac{d}{dr}(rC_{\theta se}).$$

Equations (19) and (22) now form the required two differential equations for the unknowns C_{xR} and C_{xs}. They are re-written in a non-dimensional form in Appendix 1c.

2.4 Numerical solution

This section outlines the general method of solution that has been adopted throughout. Each of the three cases considered in the previous sections yielded a set of simultaneous linear first-order differential equations.

The Runge-Kutta numerical technique for the integration of a set of first-order differential equations was chosen.

The/

The equations to be solved must be written in the form

$$\frac{d}{dr}\left(\frac{C_{x_1}}{C_{x_o}}\right) = g_1\left(R, \frac{C_{x_1}}{C_{x_o}}, \frac{C_{x_2}}{C_{x_o}}, \ldots \frac{C_{x_n}}{C_{x_o}}, \text{other factors}\right)$$

$$\frac{d}{dr}\left(\frac{C_{x_2}}{C_{x_o}}\right) = g_2\left(R, \frac{C_{x_1}}{C_{x_o}}, \ldots \quad , \quad " \quad " \right) \qquad \ldots(23)$$

$$\frac{d}{dr}\left(\frac{C_{x_3}}{C_{x_o}}\right) = g_3\left(R, \frac{C_{x_1}}{C_{x_o}}, \ldots \quad , \quad " \quad " \right)$$

where other factors include such quantities as ϕ, f, F, $\bar{\alpha}$, $\bar{\beta}$, $\bar{\gamma}$ and K. n represents the number of rows in the machine.

Numerical solutions of these equations requires an initial assumption of the values of the dependent variables at some radial station R_o (usually the geometric mean section), and a knowledge of the values of the fluid angles at exit from each blade row as a function of radius. These are known from the earlier design analysis, and are assumed to remain unchanged with flow coefficient. With the blading design chosen and the dimensions of the machine fixed, the values of the constants (K, $\bar{\alpha}$, $\bar{\beta}$, $\bar{\gamma}$) are known.

As a first approximation, values of unity for the dependent variables are assumed at radial station (R_o). When this and the values of exit fluid angles and other constants corresponding to the radial station are substituted into the set of equation (23), each of the equations will yield new values of $\frac{C_{x_1}}{C_{x_o}}, \frac{C_{x_2}}{C_{x_o}}, \ldots \frac{C_{x_n}}{C_{x_o}}$ at $R_o + \Delta R$. This process is continued and new values of $\frac{C_{x_1}}{C_{x_o}} \ldots\ldots \frac{C_{x_n}}{C_{x_o}}$ are then calculated at $R_o + 2\Delta R$ and $R_o + 3\Delta R$ and so on until the outer diameter is reached. Similarly for the inner diameter.

The final axial velocity profile behind each row of blades is thus produced. A check on the initial values that were assigned to the dependent variables is contained in the continuity condition which must be satisfied at the trailing edge of each row. Thus at any flow coefficient (ϕ), the mass flow at entry to the stage is

$$M_o = K_1\left(\frac{1 - R_h^2}{2}\right) \quad \text{where} \quad K_1 = 2\pi\rho r_t^2 C_{x_o}$$

and should be equal to the mass flow behind the n^{th} row.

M_n/

$$M_n = K_1 \int_{R_h}^{1} \frac{C_{x_n}}{C_{x_o}} R\,dR$$

if $\frac{1 - R_h^2}{2} = \lambda_o$, and the integral $\int_{R_h}^{1} \frac{C_{x_n}}{C_{x_o}} R\,dR = \lambda_n$ $(n = 1, 2, 3 \ldots)$

then a new initial value of $\frac{C_{x_i}}{C_{x_o}}$ at the mean section is taken as

$$\left(\frac{C_{x_i}}{C_{x_o}} \right)_{\substack{2nd \\ approx.}} = \frac{\lambda_o}{\lambda_1}$$

whilst the initial values of the profiles that satisfied continuity will remain as they were for the first approximation.

With new initial values, the whole calculation is carried out again, and the profiles obtained re-checked for continuity. This process, for the cases investigated, was found to be rapidly convergent and only two approximations were necessary.

By specifying the space chord ratio at all radii in the design (see Appendix 4) it was possible to obtain the nominal values of deflection (ε^*) and inlet-air angle (α^* or β^*) for each blade section. From the off-design calculations, it was possible to calculate the inlet angle (α or β) to each row at the inter-blade locations and the corresponding values of $(i - i^*) = (\alpha - \alpha^*)$ or $(\beta - \beta^*)$. The off-design performance could then be plotted on the Howell chart of $(\varepsilon/\varepsilon^*)$ against $\frac{(i - i^*)}{\varepsilon^*}$ for the local blade section.

The computer program devised for the numerical solution of the set of differential equations thus has the special feature of predicting the design and off-design performance of the compressor stage over a wide range of flows up to stall and for different aspect ratios, by the mere change of value of two quantities, namely, aspect ratio and flow coefficient.

The solution for the single stage was checked against streamline curvature calculations of the performance provided by Rolls Royce Ltd.[8].

3. Presentation and Discussion of Results

The calculations are presented in the following way:-

A - Single-stage compressor.

B - Two-stage compressor.

C - Multi-stage compressor (ultimate steady flow).

In/

In the main body of calculation (Section 3.1) a comparison between the performance of compressors of different aspect ratios (A R = 1, 2, 3) but of constant high hub/tip ratio (0·750) is given for each of the three examples A, B, C.

These comparisons are shown on two main plots:-

(i) (Trailing-edge axial velocity)/blade speed vs. non-dimensional radius, at exit from inlet guide vanes, rotor and stator, for two flow coefficients (0·662 - higher than design, 0·475 - off design).

(ii) (Incidence - nominal incidence)/nominal deflection vs. (deflection/nominal deflection), (Howell's curve), for rotor and stator, at root, mean and tip diameters, and for three flow coefficients (0·662, 0·527 - at design, 0·475).

A more detailed study is then made (in Section 3.2) of example A, the single stage:-

(a) The calculated performance of the high hub/tip ratio stage is compared with calculations based on streamline curvature analysis.

(b) Actuator-disc calculations are given for a lower hub/tip ratio stage (0·555) and for a wider range of aspect ratios (A R 1, 2, 3, 4, 5).

3.1 Aspect-ratio effects for stages of hub/tip ratio 0·750

A - Single-Stage Compressor

The "off-design" axial velocity profiles at the trailing edge of the blade rows show noticeable differences for the three aspect ratios (Fig. 4). The stator blade row receives the flow at incidences that differ with the aspect ratio (Fig. 5B). The first stall in the stage appears at the stator tip, occurring earlier for A R = 1 than for A R = 3. This later stator root stall for A R = 3 is achieved at the expense of an earlier rotor tip stall (Fig. 5A) although rotor root stall, occurring first, appears little affected by change of aspect ratio.

The difference in axial velocity profile at the trailing edge of the stator for the three aspect ratios suggests that the performance of following blade rows would be affected substantially.

B - Two-Stage Compressor

The axial velocity profiles at the trailing-edge locations of the two-stage compressor are shown in Fig. 6. The operating points on the Howell curve for each blade row (Fig. 7) show substantial aspect-ratio effects.

Stall in the two-stage machine appears to occur

(i) for low aspect ratio, at the first-stage stator tip,

(ii) for high aspect ratio, simultaneously at second stator root and all along the first stator.

There/

There are two other interesting features of the calculations:

(a) The calculations for the two-stage compressor show a definite trend for the pattern of axial velocity at blade row trailing edges to repeat in the second stage.

(b) The presence of a second stage hastens the stall of the first-stage stator and magnifies differences between the performance of compressors of different aspect ratios.

C - Multi-Stage Compressor

The "ultimate steady flow" analysis developed for the multi-stage compressor strictly applies only to deeply embedded stages of identical geometry, through which the flow pattern repeats. However the solutions obtained (Figs. 8 and 9) are similar to those for the second stage of the two-stage design. This suggests that the "ultimate steady flow" profiles are established after the stator of the first stage.

These "ultimate steady flow" profiles are different for different aspect-ratio blades. Again it appears that for the low-aspect-ratio machine, rotor tip stall is delayed at the expense of early stator tip stall.

3.2 Detailed study of single-stage performance

(i) Predictions of the axial velocities at the trailing edges of blade rows, based on actuator-disc and streamline curvature calculations, have been compared for the three aspect ratios. The maximum difference between these velocities is some 1%, and to all intents and purposes the two analyses give identical results.

(ii) For a lower hub/tip ratio (0·555), calculations were made of single-stage performance, using a wider range of aspect ratios (A R = 1, 2, 3, 4, 5). These results are presented in Fig. 10.

These results show the larger aspect-ratio effects expected in a low hub/tip ratio machine, but it is significant that the greatest differences in velocity profiles occur between A R = 1 and 2, and that the differences diminish with increasing aspect ratio.

4. Conclusions

An actuator-disc analysis for predicting the performance of single-, two- and multi-stage axial-flow compressors of varying aspect ratio is described. Calculations based on this analysis have been compared with streamline curvature calculations. The comparison shows excellent agreement between the two sets of calculations.

Results of these theoretical investigations confirm the existence of differences, small but significant, between the performance of machines of different aspect ratios. They suggest that in single-stage, two-stage and multi-stage machines of low aspect ratio, local stall first occurs at the stator tip. For higher aspect ratios, a complete stator stall (root to tip), usually occurs, although in the two-stage machine there is a tendency towards

stall/

stall of the second stator root. In general rotor stall follows stator stall, with little difference between aspect ratio, at the hub and mean regions of the blade. The rotor tip tends to stall earlier when the aspect ratio is high. These results suggest severe stator stall and early rotor tip stall in high-aspect-ratio machines and appear to be consistent with the experimental results that show the range of performance of high-aspect-ratio machines is narrower than that for low aspect ratio.

These general conclusions are emphasised in the calculations of performance of the low hub/tip ratio compressor stage.

An extension of the analysis is at present being carried out, introducing losses into the flow equations. Detailed experimental traverses on a single-stage axial-flow compressor (A R = 1 and 2) are planned in the near future.

Notation

r, θ, x	cylindrical co-ordinates (Fig. 1)
C_r	velocity in direction r
C_θ	velocity in direction θ
C_x	velocity in direction x
$R = \frac{r}{r_t}$	non-dimensional radius (= radius/tip radius)
α	fluid angle at entry or exit from a stator row (absolute) (Fig. 2)
β	fluid angle at entry or exit from a rotor row (relative) (Fig. 2)
$U = \Omega r$	blade speed (Ω, angular velocity; r, radius)
h_o	stagnation enthalpy
ψ	stream function
ϕ	flow coefficient ($= C_{x_o}/U_m$)
A R	aspect ratio (= blade height/axial chord length)
K	constant (= tip radius/mean radius)
V	non-dimensional gradient of axial velocity in r direction
f	tangent of air angle at exit from a blade row
$F = df/dR$	
ΔW	work done on the fluid by the moving blade row

M/

M	mass flow of the air
ρ	mean density of the air
$\bar{\alpha}, \bar{\beta}, \bar{\gamma}, \bar{\delta}, \bar{\omega}$	interference coefficients
x	distance from actuator disc (always positive)
ℓ	blade height
η	vorticity component in tangential direction
θ	$r.C_\theta$

Subscripts (see Fig. 3)

o	entry conditions
1, 2, 3, 4, 5	radial equilibrium conditions (that would be attained far downstream of a blade row)
01, 02, 03, 04, 05	positions of the actuator discs replacing blade rows
1e, 2e, 3e, 4e, 5e	positions of the trailing edges of blade rows
S, R	radial equilibrium conditions (case of ultimate steady flow)
OS, OR	positions of the actuator discs (case of ultimate steady flow)
Se, Re	positions of the trailing edges (case of ultimate steady flow)
t, m, h	tip, mean, hub

Appendices/

Appendices

1 - The Single-Stage Compressor

Equations (10), (11) and (12) may be expressed non-dimensionally by dividing each of these equations through by C_{x_0}, the inlet axial velocity, and replacing r, the radius, by $R(=\frac{r}{r_t})$, the non-dimensional radius. After some rearrangement, the equations become:-

for the guide vane,

$$\left[\frac{d}{dR}\left(\frac{C_{x_1}}{C_{x_0}}\right)\right]\left\{\frac{C_{x_1}}{C_{x_0}}+\frac{C_{x_{1e}}}{C_{x_0}}f_1^2\bar{\beta}_1\right\}+\left[\frac{d}{dR}\left(\frac{C_{x_2}}{C_{x_0}}\right)\right]\left\{\frac{C_{x_{1e}}}{C_{x_0}}f_1^2\bar{\gamma}_1\right\}$$

$$+\left(\frac{C_{x_{1e}}}{C_{x_0}}\right)^2 f_1\left(F_1+\frac{f_1}{R}\right)=0$$

for the rotor,

$$\left[\frac{d}{dR}\left(\frac{C_{x_1}}{C_{x_0}}\right)\right]\left\{\frac{C_{x_{2e}}}{C_{x_0}}f_2^2\bar{\beta}_2+\frac{KR}{\phi}f_1\bar{\beta}_1\right\}+\left[\frac{d}{dR}\left(\frac{C_{x_2}}{C_{x_0}}\right)\right]\left\{\frac{C_{x_2}}{C_{x_0}}+\frac{C_{x_{2e}}}{C_{x_0}}f_2^2\bar{\gamma}_2+\frac{KR}{\phi}f_1\bar{\gamma}_1\right\}$$

$$+\left[\frac{d}{dR}\left(\frac{C_{x_3}}{C_{x_0}}\right)\right]\frac{C_{x_{2e}}}{C_{x_0}}f_2^2\bar{\delta}_2+\left(\frac{C_{x_{2e}}}{C_{x_0}}\right)^2 f_2\left(F_2+\frac{f_2}{R}\right)$$

$$+\frac{KR}{\phi}\frac{C_{x_{1e}}}{C_{x_0}}\left(F_1+\frac{f_1}{R}\right)-2\frac{K}{\phi}\frac{C_{x_{2e}}}{C_{x_0}}f_2=0$$

for the stator,

$$\left[\frac{d}{dR}\left(\frac{C_{x_1}}{C_{x_0}}\right)\right]\left\{\frac{KR}{\phi}f_2^2\bar{\beta}_2+\frac{KR}{\phi}f_1\bar{\beta}_1\right\}+\left[\frac{d}{dR}\left(\frac{C_{x_2}}{C_{x_0}}\right)\right]\left\{\frac{C_{x_{3e}}}{C_{x_0}}f_3^2\bar{\gamma}_3+\frac{KR}{\phi}f_2\bar{\gamma}_2+\frac{KR}{\phi}f_1\bar{\gamma}_1\right\}$$

$$+\left[\frac{d}{dR}\left(\frac{C_{x_3}}{C_{x_0}}\right)\right]\left\{\frac{C_{x_3}}{C_{x_0}}+\frac{C_{x_{3e}}}{C_{x_0}}f_3^2\bar{\delta}_3+\frac{KR}{\phi}f_2\bar{\delta}_2\right\}$$

$$+\left(\frac{C_{x_{3e}}}{C_{x_0}}\right)^2 f_3\left(F_3+\frac{f_3}{R}\right)+\frac{KR}{\phi}\frac{C_{x_{2e}}}{C_{x_0}}\left(F_2+\frac{f_2}{R}\right)$$

$$+\frac{KR}{\phi}\frac{C_{x_{1e}}}{C_{x_0}}\left(F_1+\frac{f_1}{R}\right)-2\frac{K^2R}{\phi^2}=0$$

where $K = r_t/r_M$, $\phi = C_{x_0}/U_m$.

2 - The Two-Stage Compressor/

2 - The Two-Stage Compressor

Equations similar to those for the single-stage compressor are formed for the inlet guide vanes, first rotor, first stator, second rotor, second stator. Expressed non-dimensionally and with some rearrangement, the equations become:-

for the guide vane,

$$\left[\frac{d}{dR}\left(\frac{C_{x_1}}{C_{x_0}}\right)\right]\left\{\frac{C_{x_1}}{C_{x_0}}+\frac{C_{x_{1e}}}{C_{x_0}}f_1^2\bar{\beta}_1\right\}+\frac{d}{dR}\left(\frac{C_{x_2}}{C_{x_0}}\right)\left\{\frac{C_{x_{1e}}}{C_{x_0}}f_1^2\bar{\gamma}_1\right\}$$
$$+\left(\frac{C_{x_{1e}}}{C_{x_0}}\right)^2 f_1\left(F_1+\frac{f_1}{R}\right)=0$$

for the first rotor,

$$\left[\frac{d}{dR}\left(\frac{C_{x_1}}{C_{x_0}}\right)\right]\left\{\frac{C_{x_{2e}}}{C_{x_0}}f_2^2\bar{\beta}_2+\frac{RK}{\phi}f_1\bar{\beta}_1\right\}+\left[\frac{d}{dR}\left(\frac{C_{x_2}}{C_{x_0}}\right)\right]\left\{\frac{C_{x_2}}{C_{x_0}}+\frac{C_{x_{2e}}}{C_{x_0}}f_2^2\bar{\gamma}_2+\frac{RK}{\phi}f_1\bar{\gamma}_1\right\}$$
$$+\left[\frac{d}{dR}\left(\frac{C_{x_3}}{C_{x_0}}\right)\right]\left\{\frac{C_{x_{2e}}}{C_{x_0}}f_2^2\bar{\delta}_2\right\}+\left(\frac{C_{x_{2e}}}{C_{x_0}}\right)^2 f_2\left(F_2+\frac{f_2}{R}\right)+\frac{C_{x_{1e}}}{C_{x_0}}\frac{RK}{\phi}\left(F_1+\frac{f_1}{R}\right)$$
$$-2\frac{C_{x_{2e}}}{C_{x_0}}f_2\frac{K}{\phi}=0$$

for the first stator,

$$\left[\frac{d}{dR}\left(\frac{C_{x_1}}{C_{x_0}}\right)\right]\left\{\frac{RK}{\phi}f_2\bar{\beta}_2+\frac{RK}{\phi}f_1\bar{\beta}_1\right\}+\left[\frac{d}{dR}\left(\frac{C_{x_2}}{C_{x_0}}\right)\right]\left\{\frac{C_{x_{3e}}}{C_{x_0}}f_3^2\bar{\gamma}_3+\frac{RK}{\phi}f_2\bar{\gamma}_2+\frac{RK}{\phi}f_1\bar{\gamma}_1\right\}$$
$$+\left[\frac{d}{dR}\left(\frac{C_{x_3}}{C_{x_0}}\right)\right]\left\{\frac{C_{x_3}}{C_{x_0}}+\frac{C_{x_{3e}}}{C_{x_0}}f_3^2\bar{\delta}_3+\frac{RK}{\phi}f_2\bar{\delta}_2\right\}+\left[\frac{d}{dR}\left(\frac{C_{x_4}}{C_{x_0}}\right)\right]\left\{\frac{C_{x_{3e}}}{C_{x_0}}f_3^2\bar{\omega}_3\right\}$$
$$+\left(\frac{C_{x_{3e}}}{C_{x_0}}\right)^2 f_3\left(F_3+\frac{f_3}{R}\right)+\frac{RK}{\phi}\frac{C_{x_{2e}}}{C_{x_0}}\left(F_2+\frac{f_2}{R}\right)+\frac{RK}{\phi}\frac{C_{x_{1e}}}{C_{x_0}}\left(F_1+\frac{f_1}{R}\right)$$
$$-2R\left(\frac{K}{\phi}\right)^2=0$$

for/

for the second rotor,

$$\left[\frac{d}{dR}\left(\frac{C_{x_2}}{C_{x_o}}\right)\right]\left\{\frac{RK}{\phi} f_3 \bar{y}_3\right\} + \left[\frac{d}{dR}\left(\frac{C_{x_3}}{C_{x_o}}\right)\right]\left\{\frac{C_{x_{4e}}}{C_{x_o}} f_4^2 \bar{\delta}_4 + \frac{RK}{\phi} f_3 \bar{\delta}_3\right\}$$

$$+\left[\frac{d}{dR}\left(\frac{C_{x_4}}{C_{x_o}}\right)\right]\left\{\frac{C_{x_4}}{C_{x_o}} + \frac{C_{x_{4e}}}{C_{x_o}} f_4^2 \bar{\omega}_4 + \frac{RK}{\phi} f_3 \bar{\omega}_3\right\} + \left[\frac{d}{dR}\left(\frac{C_{x_5}}{C_{x_o}}\right)\right]\left\{\frac{C_{x_{4e}}}{C_{x_o}} f_4^2 \bar{\psi}_4\right\}$$

$$+\left(\frac{C_{x_{4e}}}{C_{x_o}}\right)^2 f_4\left(F_4 + \frac{f_4}{R}\right) + \frac{C_{x_{3e}}}{C_{x_o}} \frac{RK}{\phi}\left(F_3 + \frac{f_3}{R}\right) - 2\frac{C_{x_{4e}}}{C_{x_o}} f_4 \frac{K}{\phi} = 0$$

for the second stator,

$$\left[\frac{d}{dR}\left(\frac{C_{x_2}}{C_{x_o}}\right)\right]\left\{\frac{RK}{\phi} f_3 \bar{y}_3\right\} + \left[\frac{d}{dR}\left(\frac{C_{x_3}}{C_{x_o}}\right)\right]\left\{\frac{RK}{\phi} f_4 \bar{\delta}_4 + \frac{RK}{\phi} f_3 \bar{\delta}_3\right\}$$

$$+\left[\frac{d}{dR}\left(\frac{C_{x_4}}{C_{x_o}}\right)\right]\left\{\frac{C_{x_{5e}}}{C_{x_o}} f_5 \bar{\omega}_5 + \frac{RK}{\phi} f_4 \bar{\omega}_4 + \frac{RK}{\phi} f_3 \bar{\omega}_3\right\}$$

$$+\left[\frac{d}{dR}\left(\frac{C_{x_5}}{C_{x_o}}\right)\right]\left\{\frac{C_{x_5}}{C_{x_o}} + \frac{C_{x_{5e}}}{C_{x_o}} f_5^2 \bar{\psi}_5 + \frac{RK}{\phi} f_4 \bar{\psi}_4 + \frac{RK}{\phi} f_3 \bar{\psi}_3\right\}$$

$$+\left(\frac{C_{x_{5e}}}{C_{x_o}}\right)^2 f_5\left(F_5 + \frac{f_5}{R}\right) + \frac{RK}{\phi}\frac{C_{x_{4e}}}{C_{x_o}}\left(F_4 + \frac{f_4}{R}\right) + \frac{RK}{\phi}\frac{C_{x_{3e}}}{C_{x_o}}\left(F_3 + \frac{f_3}{R}\right)$$

$$- 2R\left(\frac{K}{\phi}\right)^2 = 0.$$

3 - The Multi-Stage Compressor

The two differential equations in their final non-dimensional form are:

Equation (22)

$$\left[\frac{d}{dR}\left(\frac{C_{x_S}}{C_{x_o}}\right)\right]\left\{\frac{C_{x_S}}{C_{x_o}} + Pf_2 \frac{KR}{\phi} - Pf_2^2 \frac{C_{x_{Re}}}{C_{x_o}} + Qf_1^2 \frac{C_{x_{Se}}}{C_{x_o}}\right\}$$

$$+\left[\frac{d}{dR}\left(\frac{C_{x_R}}{C_{x_o}}\right)\right]\left\{-\frac{C_{x_R}}{C_{x_o}} + QKf_2 \frac{R}{\phi} - Qf_2^2 \frac{C_{x_{Re}}}{C_{x_o}} + Pf_1^2 \frac{C_{x_{Se}}}{C_{x_o}}\right\}$$

$$= \left(\frac{K}{\phi} - \frac{f_2}{R}\frac{C_{x_{Re}}}{C_{x_o}}\right)\left\{2\frac{RK}{\phi} - RF_2 \frac{C_{x_{Re}}}{C_{x_o}} - \frac{C_{x_{Re}}}{C_{x_o}} f_2\right\} - \frac{C_{x_{Se}}}{C_{x_o}}\frac{f_1}{R}\left\{RF_1 \frac{C_{x_{Se}}}{C_{x_o}} + f_1 \frac{C_{x_{Se}}}{C_{x_o}}\right\}$$

Equation (19)/

Equation (19)

$$\left[\frac{d}{dR}\left(\frac{C_{xS}}{C_{x_o}}\right)\right]\{PRf_2 + QRf_1\} + \left[\frac{d}{dR}\left(\frac{C_{xR}}{C_{x_o}}\right)\right]\{QRf_2 + PRf_1\}$$

$$= 2\frac{RK}{\phi} - \frac{C_{xRe}}{C_{x_o}}\{RF_2 + f_2\} - \frac{C_{xSe}}{C_{x_o}}\{RF_1 + f_1\}$$

where

$$f_1 = \tan\alpha_e, \qquad f_2 = \tan\beta_e$$

$$F_1 = \frac{d}{dR}f_1, \qquad F_2 = \frac{d}{dR}f_2, \qquad K = \frac{r_t}{r_m}$$

and

$$C_{xSe} = QC_{xS} + PC_{xR}$$

$$C_{xRe} = QC_{xR} + PC_{xS}$$

where

$$P = e^{-\pi\frac{x}{\ell}}, \qquad Q = 1 - P.$$

4 - Air Angles at Exit from the Blade Rows - The design values are presented as functions of radius (R) and space-chord (S/C). These values are also used off design in the high hub/tip ratio calculations.

			Air angle at exit from:			
R	S/C	I.G.V.	Rotor 1	Stator 1	Rotor 2	Stator 2
0·750	0·754	25·6°	12·1°	24·9°	12·0°	25·2°
0·800	0·804	27·4°	19·3°	27·0°	19·2°	27·2°
0·850	0·854	29·2°	26·4°	29·0°	26·4°	29·1°
0·900	0·904	30·9°	33·3°	31·0°	33·3°	30·9°
0·950	0·955	32·5°	39·8°	33·1°	39·9°	32·8°
1·000	1·005	34·2°	45·9°	35·2°	46·0°	34·7°

These values were extrapolated for the low hub/tip ratio stage.

References/

References

No.	Author(s)	Title, etc.
1	J. H. Horlock, R. Shaw, D. Pollard and A. Lewkowicz	Reynolds number effects in cascades and axial flow compressors. Journal of Engineering for Power, Vol.86, Series A, pp.236-242, July, 1964.
2	J. C. Emery, L. J. Herrig and J. R. Erwin	Systematic two-dimensional tests of NACA 65-Series compressor blades at low speeds. NACA TN-3916, 1957.
3	W. C. Swan	An experiment with aspect ratio as a means of extending the useful range of a transonic inlet stage of an axial flow compressor. Journal of Engineering for Power, Vol.86, Series A, pp.243-246, July, 1964.
4	L. H. Smith, Jr., S. C. Traugott and G. F. Wislicenus	A practical solution of a three-dimensional flow problem of axial turbomachinery. Trans ASME - 75, pp.789-803, 1953.
5	W. R. Hawthorne and J. H. Horlock	Actuator disc theory of the incompressible flow in axial compressors. Proc. I. Mech. E., 176, No.30, 789, 1962.
6	J. H. Horlock	Axial flow compressors. Butterworths Scientific Publications 1958.
7	J. H. Horlock	Communication relating to the paper "Three-Dimensional Design of Multi-Stage Axial Flow Compressors" by J. W. Railly. J. Mech. Eng. Sci. 3, No.3, 286, 1961.
8	R. Hetherington and M. E. Silvester	Computation of compressor performance including the effects of hade and streamline curvature. T.G.R. No.90002, Internal Report, Rolls Royce Ltd., Derby.

HD

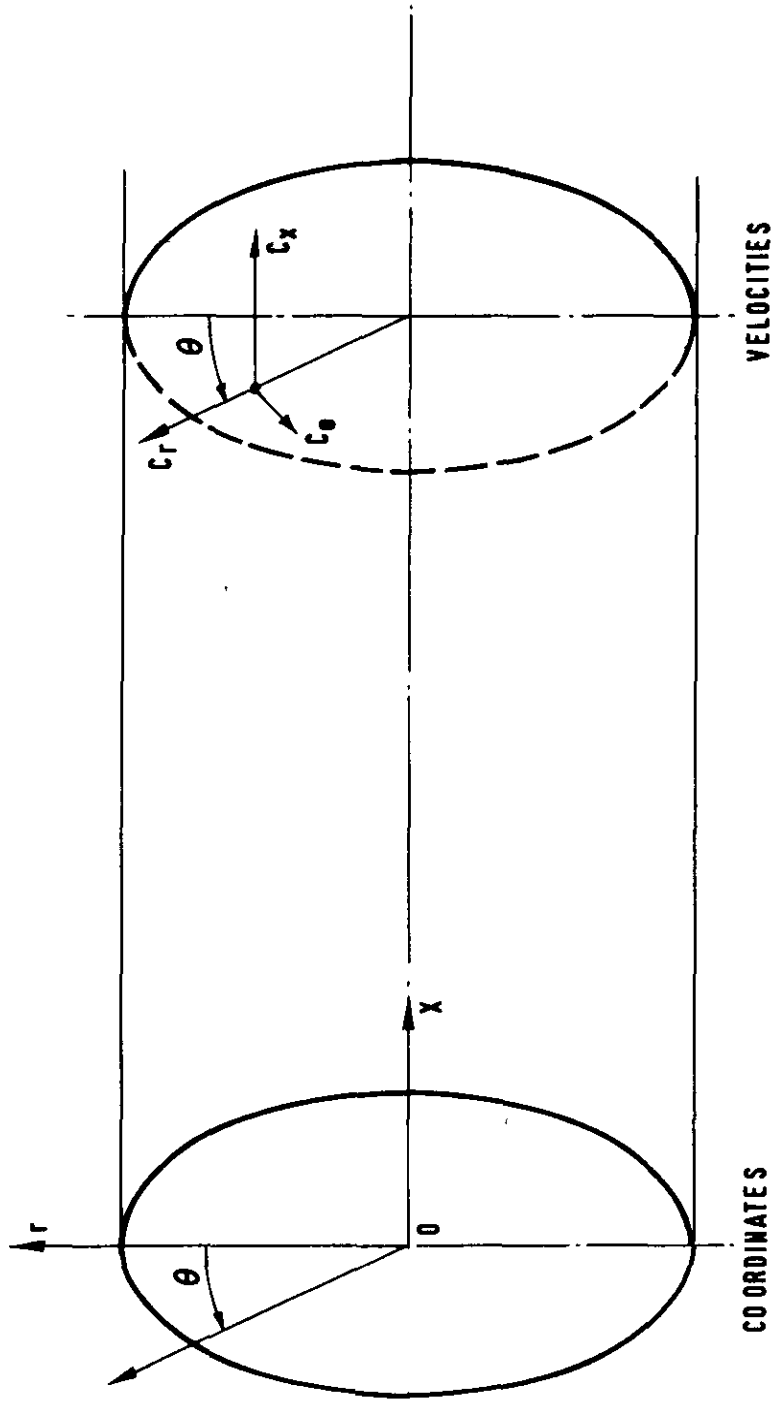

FIG 1 COORDINATE SYSTEM

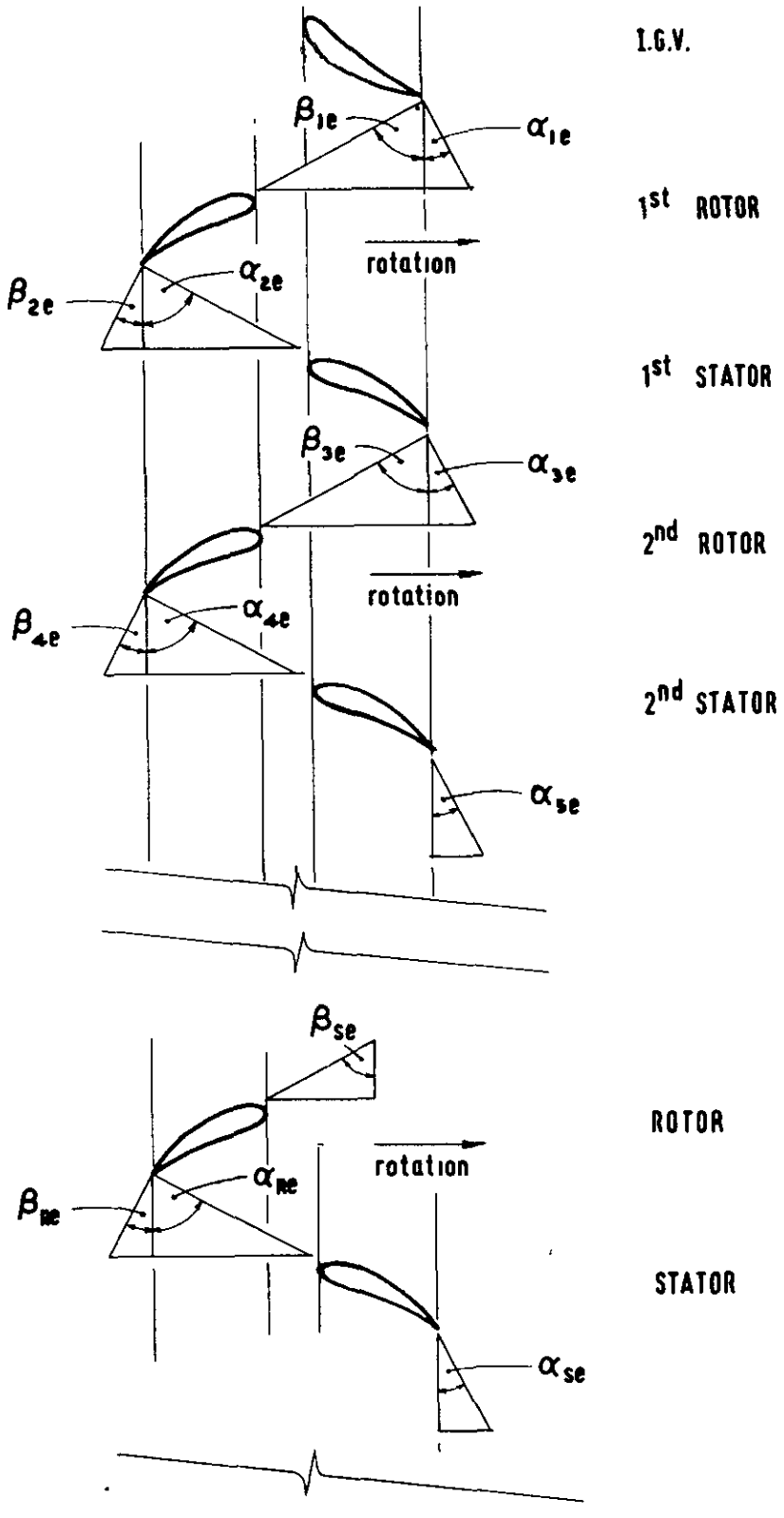

FIG 2 AIR ANGLE NOTATION

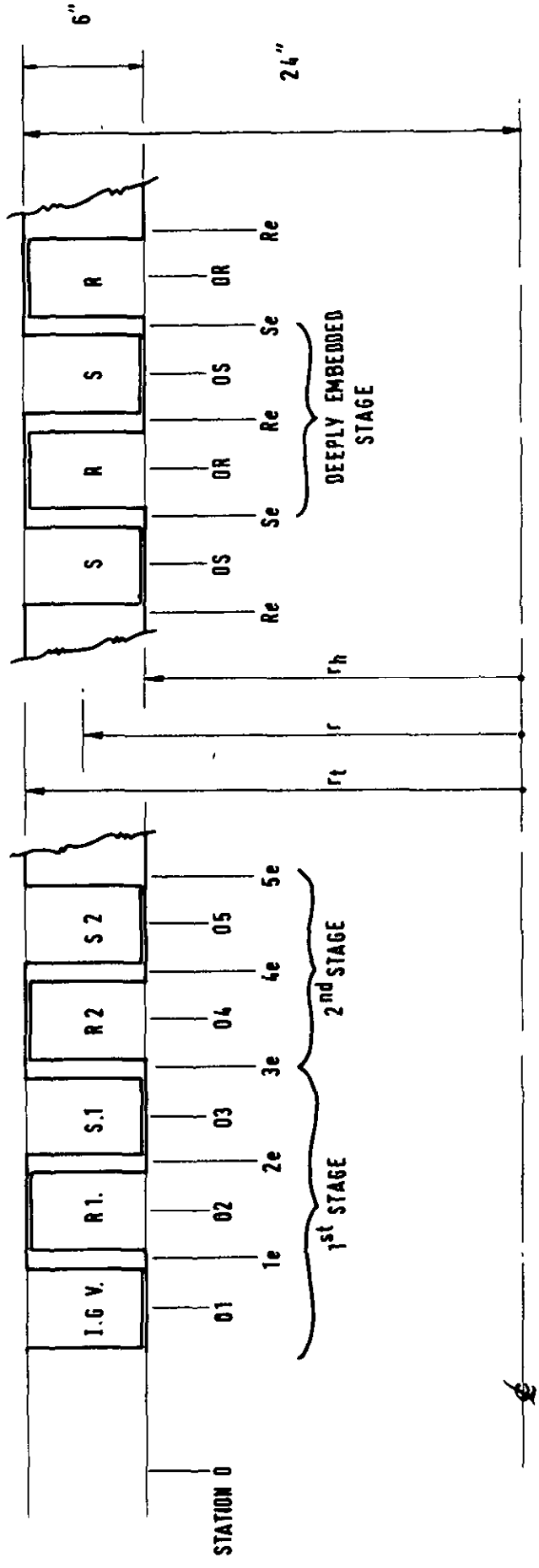

FIG. 3 ACTUATOR DISC AND TRAILING EDGE STATIONS FOR THE SYSTEMS ANALYSED

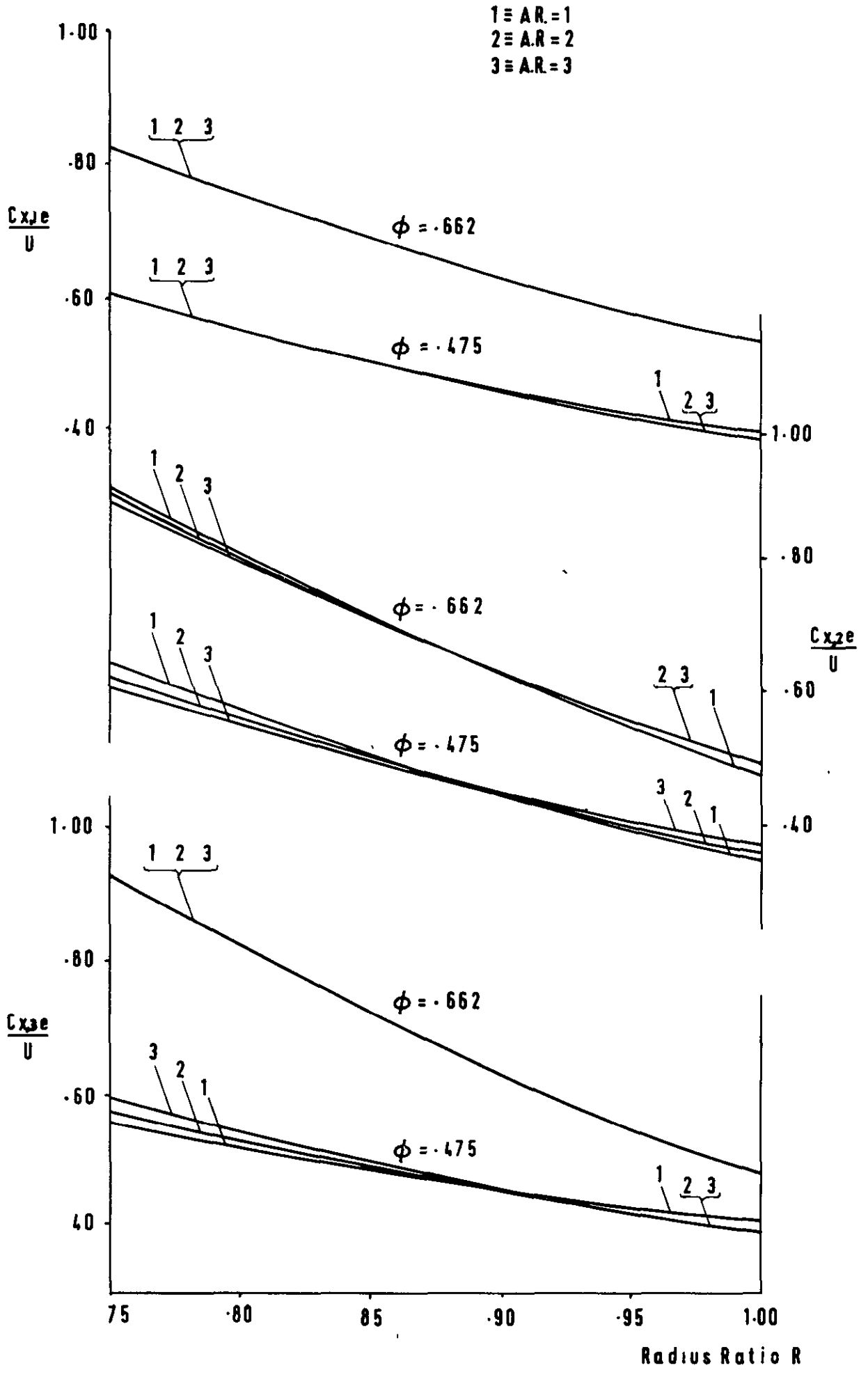

FIG.4 PREDICTED VELOCITY PROFILES FOR SINGLE-STAGE COMPRESSOR

FIGS.5a,b PREDICTED OPERATING POINTS FOR SINGLE-STAGE COMPRESSOR, PLOTTED ON HOWELL'S CURVES

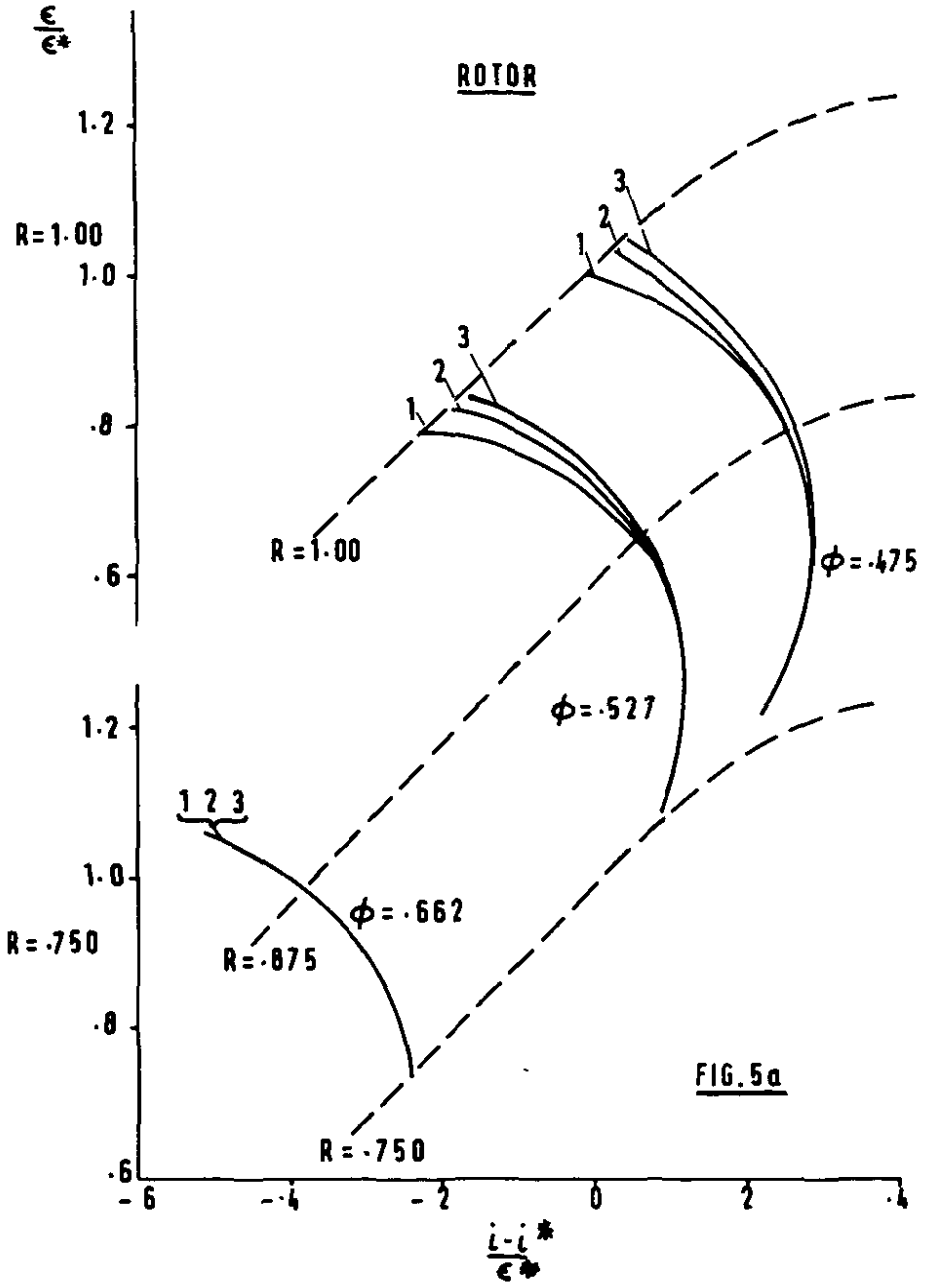

FIG.5a

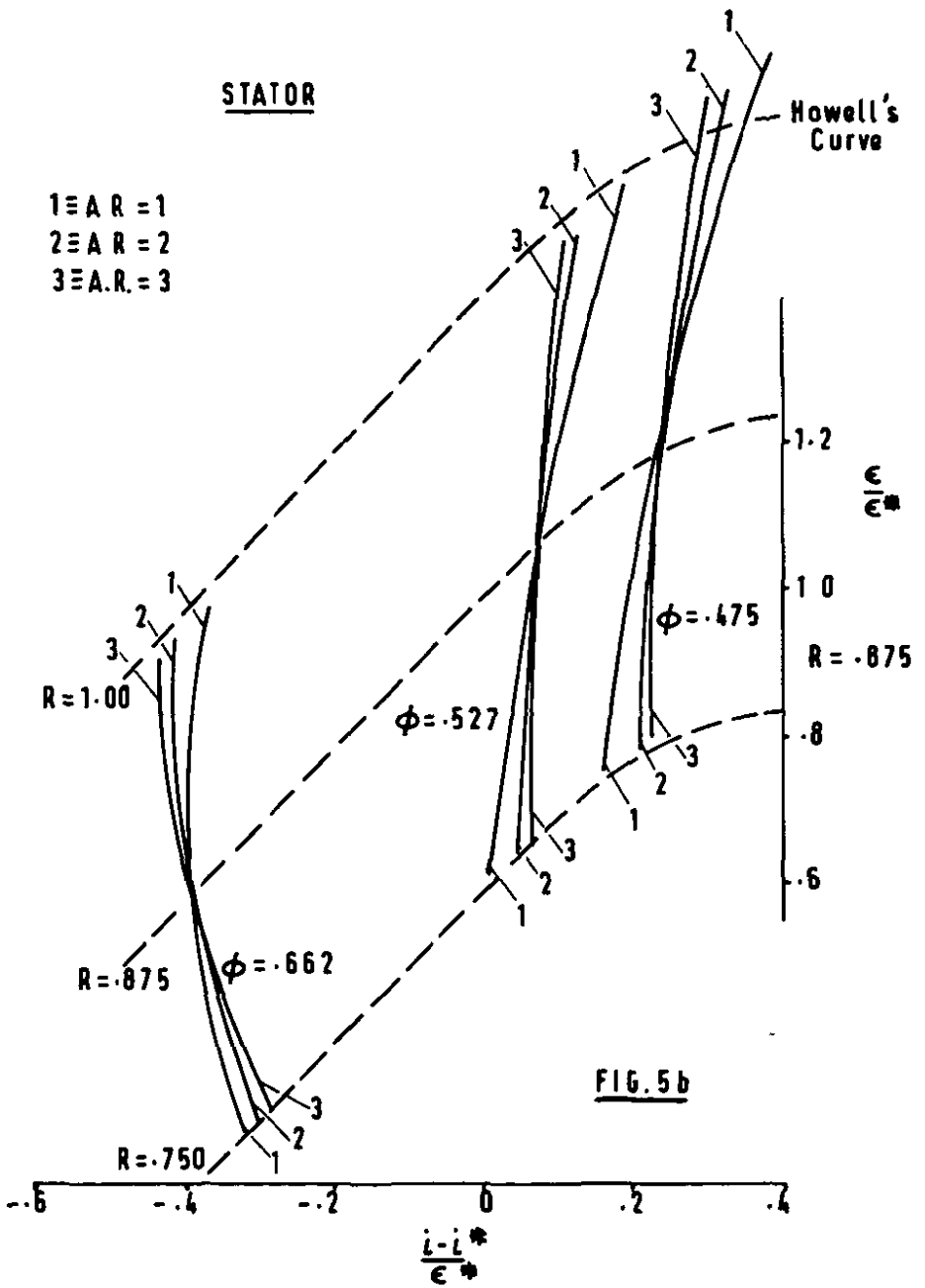

FIG.5b

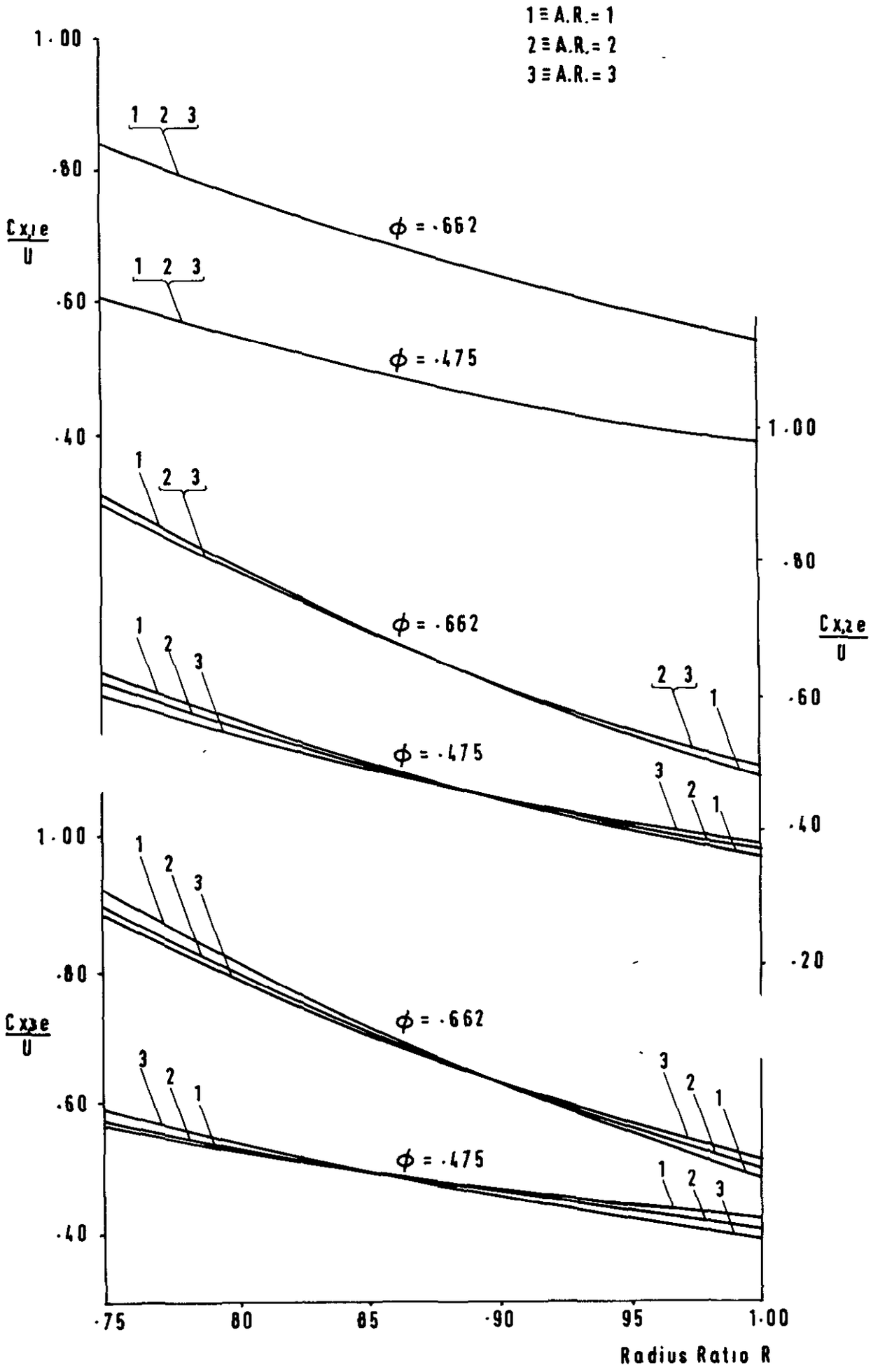

FIG.6a PREDICTED VELOCITY PROFILES FOR STAGE 1 OF TWO-STAGE COMPRESSOR

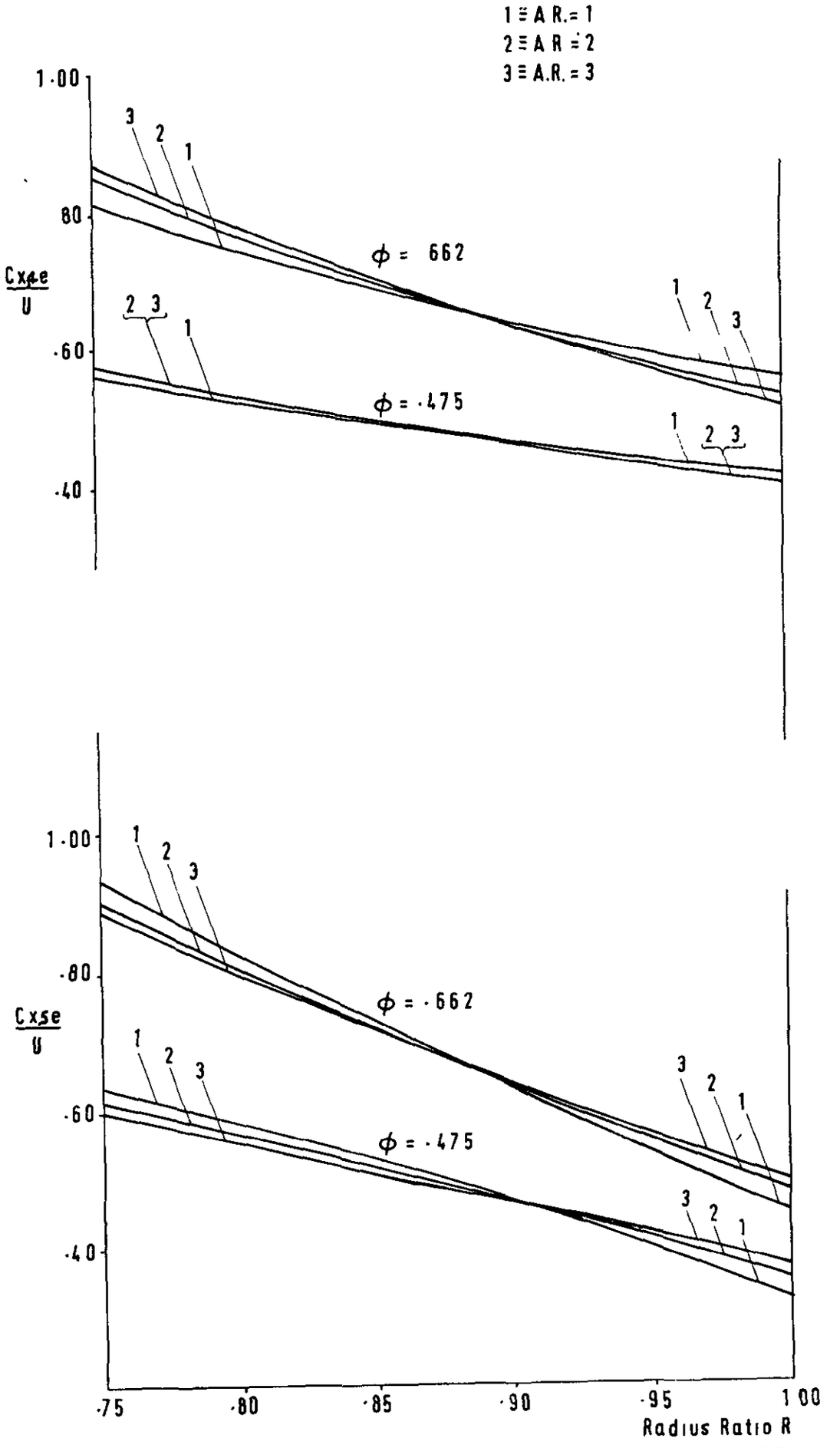

FIG.6b PREDICTED VELOCITY PROFILES FOR STAGE 2 OF TWO-STAGE COMPRESSOR

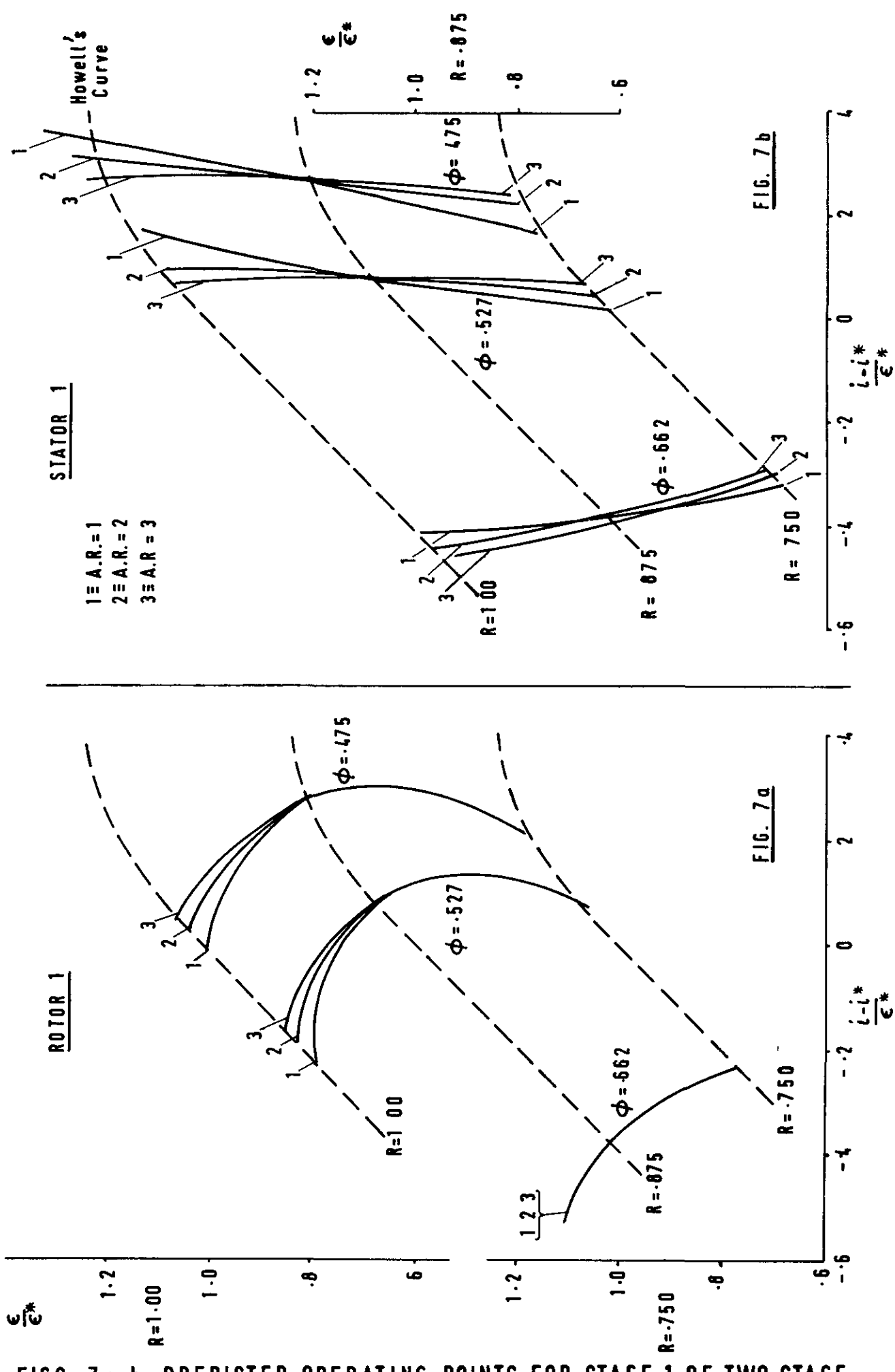

FIGS. 7a.b. PREDICTED OPERATING POINTS FOR STAGE 1 OF TWO-STAGE COMPRESSOR, PLOTTED ON HOWELL'S CURVES

FIGS. 7 c.d. PREDICTED OPERATING POINTS FOR STAGE 2 OF TWO-STAGE COMPRESSOR, PLOTTED ON HOWELL'S CURVES

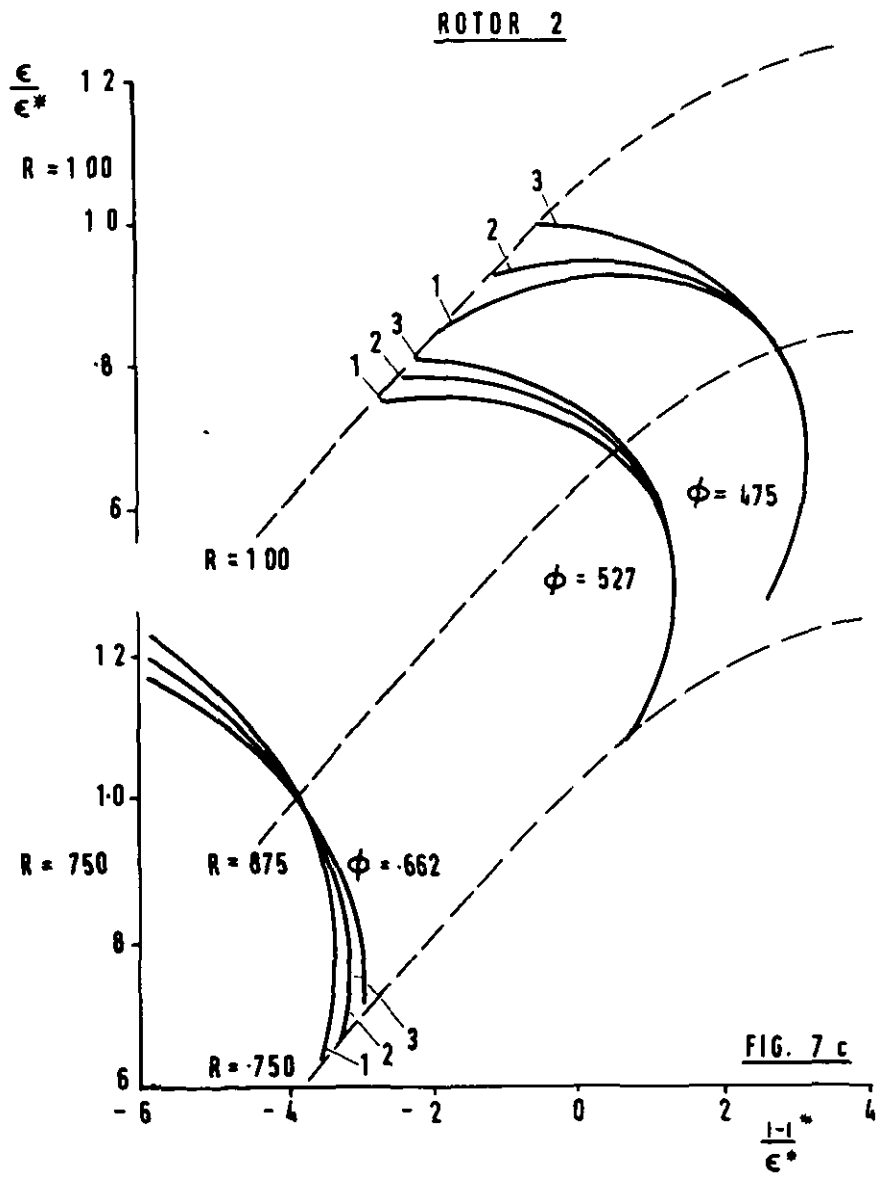

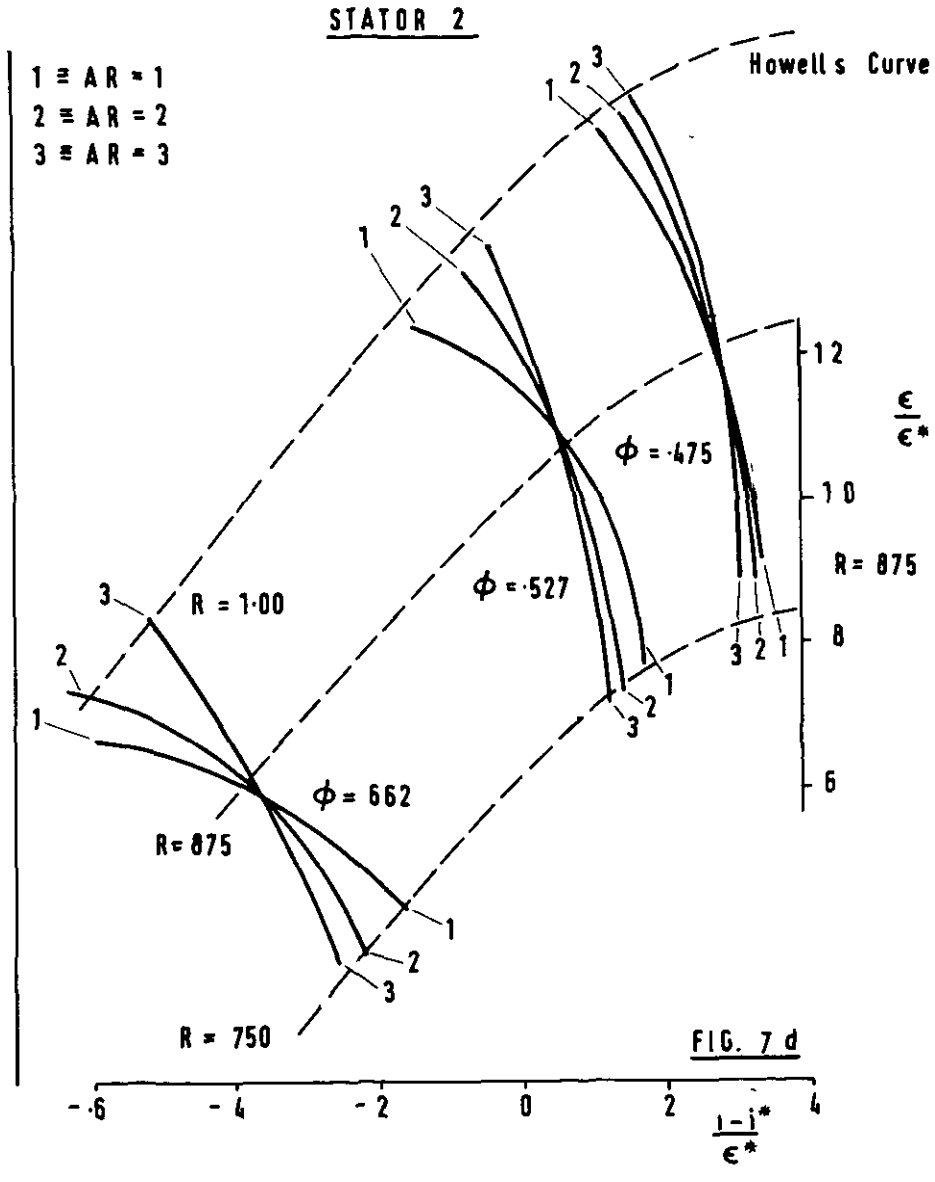

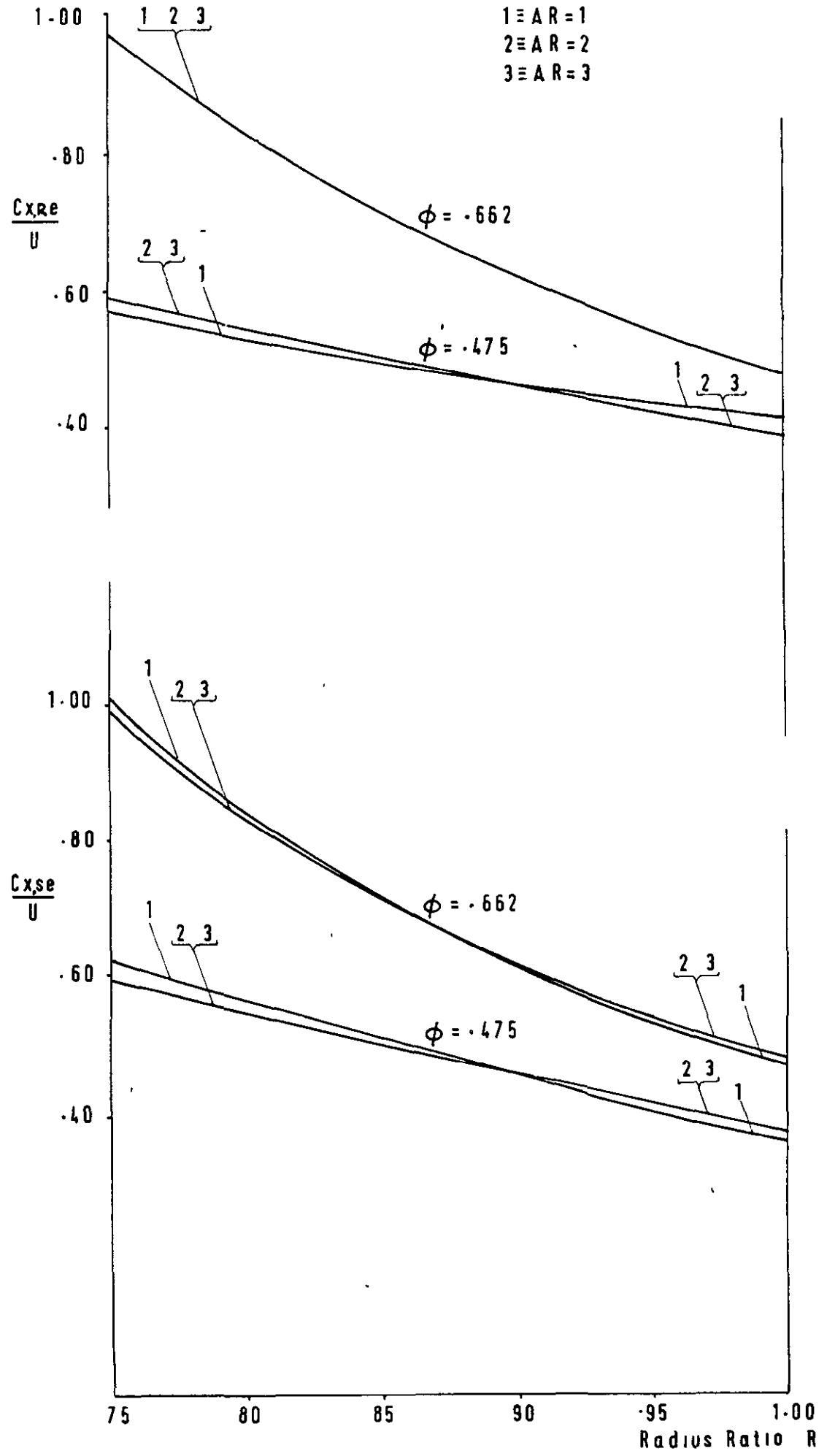

FIG.8 PREDICTED VELOCITY PROFILES FOR EMBEDDED STAGE OF MULTI-STAGE COMPRESSOR

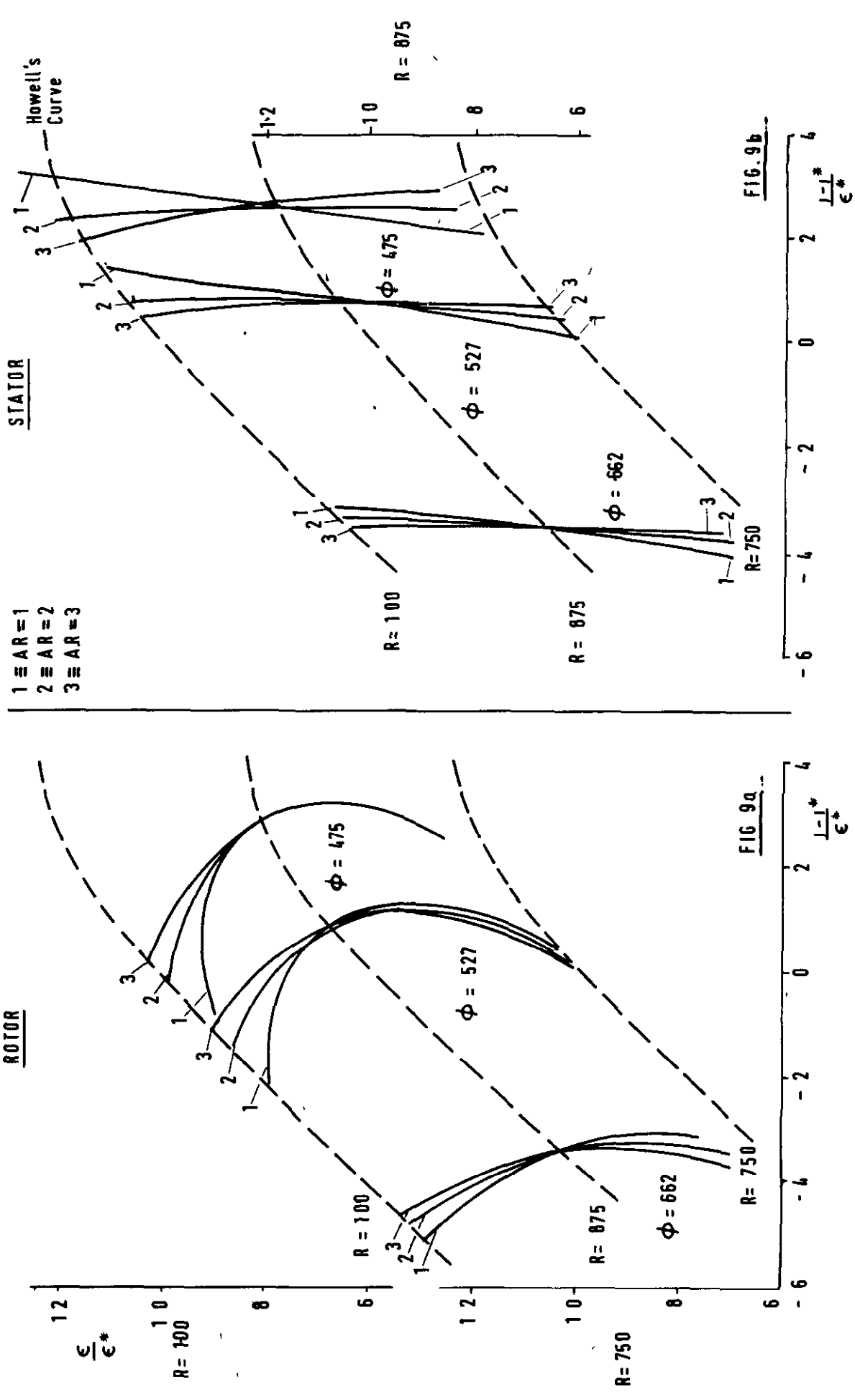

FIGS. 9 a, b. PREDICTED OPERATING POINTS FOR EMBEDDED STAGE OF MULTI-STAGE COMPRESSOR, PLOTTED ON HOWELL'S CURVES

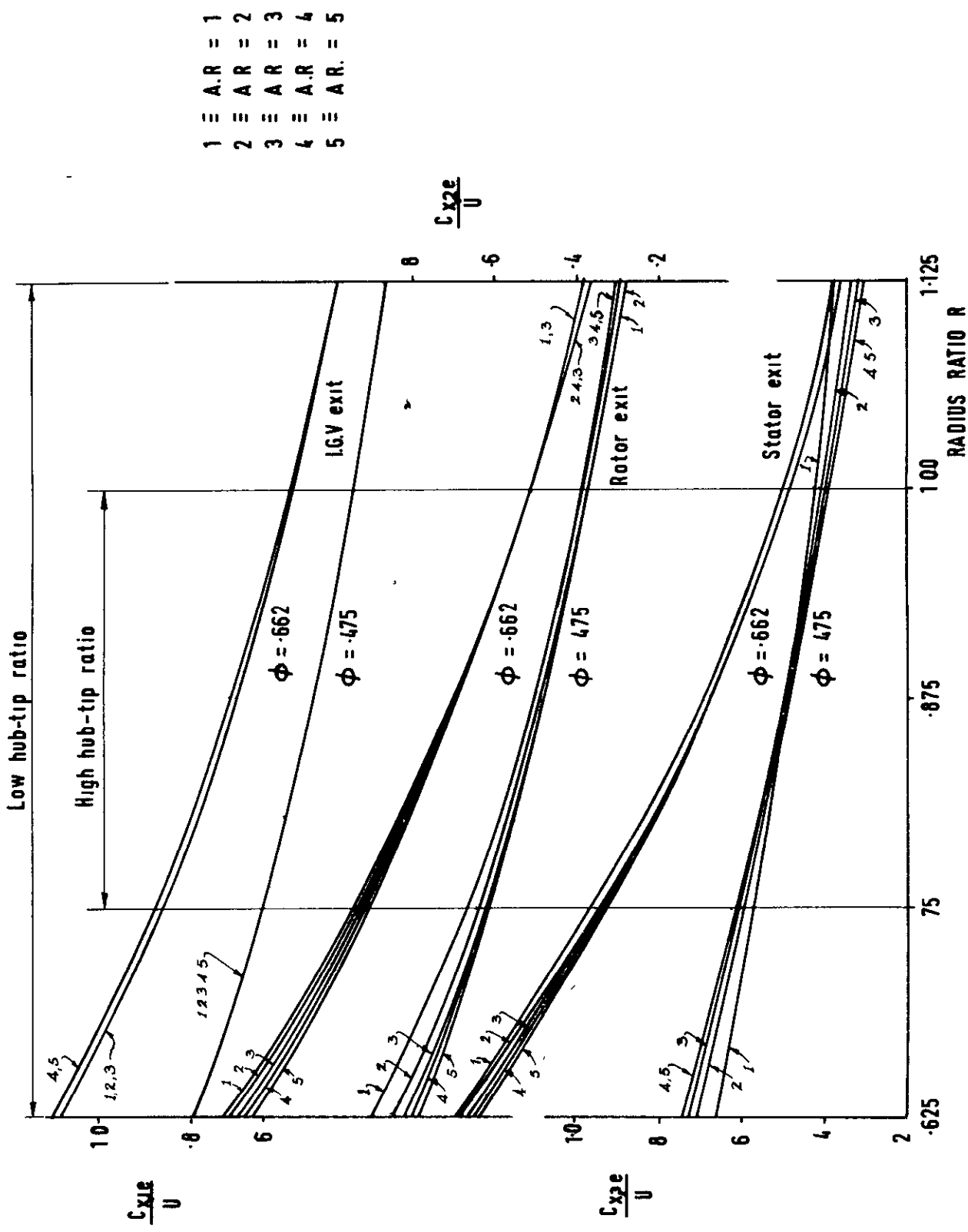

FIG.10 PREDICTED VELOCITY PROFILES FOR LOW HUB-TIP RATIO SINGLE-STAGE COMPRESSOR

C.P.943
May, 1966
Horlock, J.H. and Fahmi, G.J.

A THEORETICAL INVESTIGATION OF THE EFFECT OF ASPECT RATIO ON AXIAL FLOW COMPRESSOR PERFORMANCE

The performance of axial flow compressors is known to be affected by the choice of aspect ratio (the ratio of blade height to axial chord length). An analysis of the inviscid, incompressible flow in axial compressors of different aspect ratios is given in this paper. The main analysis is based on actuator disc theory, but a comparison is made between calculations based on this theory and the more recently developed streamline curvature analysis. This comparison shows close agreement between the calculations based on the two theories.

C.P.943
May, 1966
Horlock, J.H. and Fahmi, G.J.

A THEORETICAL INVESTIGATION OF THE EFFECT OF ASPECT RATIO ON AXIAL FLOW COMPRESSOR PERFORMANCE

The performance of axial flow compressors is known to be affected by the choice of aspect ratio (the ratio of blade height to axial chord length). An analysis of the inviscid, incompressible flow in axial compressors of different aspect ratios is given in this paper. The main analysis is based on actuator disc theory, but a comparison is made between calculations based on this theory and the more recently developed streamline curvature analysis. This comparison shows close agreement between the calculations based on the two theories.

C.P.943
May, 1966
Horlock, J.H. and Fahmi, G.J.

A THEORETICAL INVESTIGATION OF THE EFFECT OF ASPECT RATIO ON AXIAL FLOW COMPRESSOR PERFORMANCE

The performance of axial flow compressors is known to be affected by the choice of aspect ratio (the ratio of blade height to axial chord length). An analysis of the inviscid, incompressible flow in axial compressors of different aspect ratios is given in this paper. The main analysis is based on actuator disc theory, but a comparison is made between calculations based on this theory and the more recently developed streamline curvature analysis. This comparison shows close agreement between the calculations based on the two theories.

DETACHABLE ABSTRACT CARDS

Printed and published by
HER MAJESTY'S STATIONERY OFFICE
To be purchased from
49 High Holborn, London W C 1
423 Oxford Street, London W.1
13A Castle Street, Edinburgh 2
109 St Mary Street, Cardiff
Brazennose Street, Manchester 2
50 Fairfax Street, Bristol 1
35 Smallbrook, Ringway, Birmingham 5
7 - 11 Linenhall Street, Belfast 2
or through any bookseller

Printed in England

S O Code No 23-9017-43